NANO EXPRESS

PAPER

# Effect of nanofiller morphology on the electrical conductivity of polymer nanocomposites

Qichen Fang[1,*] and Khalid Lafdi[1,2]

[1] Chemical and Materials Engineering Department University of Dayton, Dayton, OH 45469-United States of America
[2] Department of Mechanical and Construction Engineering, Northumbria University, Newcastle upon Tyne, United Kingdom
* Author to whom any correspondence should be addressed.

**E-mail:** qichenff@gmail.com

**Keywords:** conductive network, silver nanofiller, nanocomposite

Supplementary material for this article is available online

OPEN ACCESS

RECEIVED
11 December 2020

REVISED
16 January 2021

ACCEPTED FOR PUBLICATION
29 January 2021

PUBLISHED
10 February 2021



## Abstract

Conductive polymers and nanocomposites have attracted great attention in industry and academia for their tremendous potential applications. Most of the research was focused on the type and amount of nano-additives used and fewer on their morphology which is critical in forming the conductive network. In this paper, a detailed investigation of the effect nanomaterial's morphology was carried out to study their electrical conductivity properties. Silver nanowire (AgNW) nanocomposite and silver nanoparticle (AgNP) nanocomposite were fabricated. The morphology, crystallinity, and orientation of various silver nanofillers were characterized. AgNW based nanocomposites have shown a lower percolation threshold. A conductive unit based model was established to explain the evolution of the conductive network and aggregation. The aggregation geometry of nanofiller appeared as a dominant factor in altering the percolation behavior.

## 1. Introduction

Conductive polymer nanocomposites exhibit excellent electrical conductivity [1, 2] and lightweight [3], which have attracted great interest to be used as strain sensor [4, 5], biosensors [6], transparent electrodes [7–9], and surface-enhanced Raman scattering (SERS) for plasmonic applications [10]. Conductive nanofiller played an essential role in affecting nanocomposite conductivity. For silver-based nanofiller, the significant difference in structural and geometrical features between different nanofiller will bring distinct differences in nanofiller network structure and thus the nanocomposites' electrical conductivity. Two types of silver-based nanomaterials were intensively studied: silver nanoparticle (AgNP) with spherical shape and silver nanowire (AgNW) with cylindrical morphology. Recently, AgNW has been studied for the flexible transparent thin film [11–16]. The major differences between AgNP and AgNW are their geometry and specific surface area.

Silver nanomaterials can be easily synthesized by a simple polyol reduction process [17–20]. Depending on reactants concentration [21], thermal condition [22], and the stirring rate [23–25]. The geometry and aspect ratio can be well controlled [26]. AgNP can be considered as a zero-dimensional material. The diameter ranges from 5 nm to 200 nm [27–29]. AgNW is a typical one-dimensional cylindrical rod. The diameter varies from 20 nm to 200 nm, and its aspect ratio ranges from 100 to 2000 based on synthesis conditions [30–32]. As a result, AgNP has a much higher specific surface area than AgNW, and it is easier for AgNW to form a conductive network [33]. The distribution of nanoparticles can be highly affected by the process method [34], thus easily affect the network. The formation of a conductive network is the key in nanocomposite based conductive applications, such as flexible electronics, sensors, electromagnetic interference shielding [35–37]. In conductive nanowire based nanocomposites, the interactions between nanowire and matrix and their dispersion are critical for establishing an active conductive network pathway.

Soheil *et al* studied the effect of nano additive geometry in carbon-based materials. They compared multiwall carbon nanotube (MWCNT) and graphene nanoribbon (GNR) nanocomposites and found that GNR

nanocomposites have lower conductivity than MWCNT nanocomposite since GNR cannot interlace between each other tightly [38]. Nuha *et al* showed that the carbon nanotube (CNT) based nanocomposites have a much higher conductivity than the carbon black (CB) one at the same concentrations [39]. Hongjin mentioned that AgNP could enhance silver-based nanocomposite conductivity by creating a more conductive path [40]. The alignment of nanowires is an important parameter as well. Silver nanowire conductive films can have a dominant alignment by controlling viscosity and evaporation rate [41].

Computational modeling is an alternative way to understand and predict the property of derived nanocomposites [42, 43]. With the help of supercomputing methods in recent years, realistic simulation of large scale and multi-body problems becomes faster and more accessible, such as modeling the formation of a percolation network. Xiao *et al* developed a model to explain the percolation characteristics of ZnO nanoparticle in composite dielectrics. The model illustrates the formation of the conductive pathway in nanocomposite [43]. In Takuya's study, a novel morphological model was used to understand the importance of CNT aggregation and electron tunneling [44]. The effect of electron tunneling in nanocomposite's conductivity was dominant. Bao *et al* clarified that the electron tunneling was affected by polymer film's thickness between nanofiller, thus the contact resistance [45]. In Daewoo Suh's study, after adjusting the distance between silver and silicone and enabled the electron tunneling, nanocomposite's electrical conductivity increased by ~5 orders of magnitude without nanofiller's coalescence [46]. Nuha *et al* systematically studied the effect of carbon nanofiller's geometry, aspect ratio, aggregation, and concentration. Their modeling result shows that the conductivity evolution versus nano-additive concentration is profoundly affected by the degree of aggregation. They also revealed that well-dispersed nanofillers are not always preferred for the formation of conductive networks. However, the threshold percolation measured is in a vertical direction rather than an in-plane direction. The effect of the nanowire's anisotropic distribution was not well modeled, and the mechanism of particle aggregation's effect was not well illustrated [39].

In this study, the effect of different nanofillers on the formation of conductive networks in an in-plane direction was compared experimentally and numerically. Nanocomposite films were made using the spin coating method. To study the distribution of nanofillers in nanocomposite, the crystallinity and orientation of different silver nanofillers were measured using x-ray diffraction (XRD) methods. A numerical simulation was carried out to better understand the effect of nanofillers' geometry and concentration. A conductive unit based model was established to expound the effect of size and aggregation geometry on the evolution of the conductive network.

## 2. Experimental section

### 2.1. Materials

Polyacrylonitrile (PAN, acrylonitrile-co-methyl acrylate copolymer, acrylonitrile content 94%, Mw = 100000) was purchased from Scientific Polymer Inc. N, N-Dimethylformamide (DMF, anhydrous, ⩾99.8%), Anhydrous ethylene glycol (EG, ⩾99.8%), silver nitrate (AgNO3, Reagent plus, ⩾99.0%), Polyvinylpyrrolidone (PVP, powder, MW = 55000) were purchased from Sigma-Aldrich. Acetone was purchased from Alfa Aesar. Copper (II) Chloride Dihydrate ($CuCl_2$, ⩾99.8%) was purchased from Acros Organics. All chemicals were used with no further purification.

### 2.2. Preparation of AgNWs and AgNPs

AgNWs and AgNPs were synthesized separately by a polyol reduction method. In the AgNWs synthesis, 150 ml EG was added in a 250 ml three flask and heated at 150 ℃ by flask heating mantles. The stir bar was then added with a spin rate of 260 rpm. A thermometer was used at various times to measure the solution's temperature. At 1.5 h, 0.16 ml of $CuCl_2$ solution (20 mM, in EG) was added in the flask. After 20 min, 5 ml of PVP solution (0.882 M, in EG) was injected into a heated solution, followed by 5 ml of $AgNO_3$ solution (0.564 M, in EG). The reaction ended at 1.5 h, and the solution was cooled at room temperature. 100 ml Acetone was added to the product to dilute the solution. Furthermore, the products were centrifuged at 4000 rpm for 30 min. After washing the products twice with acetone, the final AgNWs were stored in acetone. Acetone can prevent the aggregation of AgNWs and will participate in the manufacturing of conductive composite. The synthesis of AgNPs was carried out similarly. The major difference was that no $CuCl_2$ was added, the PVP concentration was 0.932 M in EG, and the concentration of $AgNO_3$ was 0.72 M in EG.

### 2.3. Preparation of PAN nanocomposite

The weight of the nanofiller was well controlled. Before mixing the nanofiller with PAN, 1 g PAN was added in 9 g DMF. With a stir bar added, the PAN/DMF solution was stirred while maintaining a temperature of 65 ℃. After 12 h, the solution of PAN/DMF was well prepared. For a 20 vol% mixture of silver nanofiller and PAN, 0.6

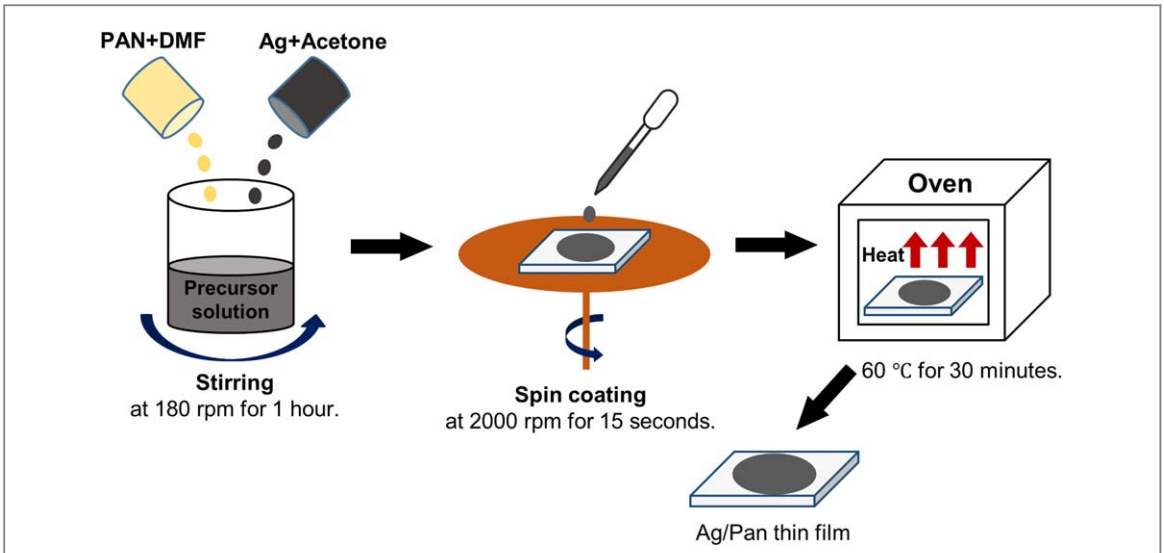


**Figure 1.** Schematic illustration of the preparation of the Ag/PAN thin film.

g of silver nanofiller was added. The silver nanofiller was soaked in acetone, and the silver precipitated after 1 min. Then 2.7 g of PAN/DMF solution was added using a pipette. By weighting the final solution, more acetone could be added to adjust the weight ratio of PAN and DMF to be 1:2. In the final mixture, there was 0.6 g of silver nanofiller, 0.27 g of PAN, 2.43 g of DMF, and 1.22 g of acetone. After stirring at 180 rpm for 1 h, a homogenous solution was obtained. The formation of aggregates could occur if the stirring time was too long. The dispersed solution was used right after the preparation. A Speed line P2604 spin coater was used to fabricate the thin film. 0.2 ml dispersed solution was added on the glass and then spun at 2000 rpm for 15 s. After the spin coater stopped, the thin film was transferred to a 60 ℃ oven immediately. After 30 min, a well-cured film was obtained. The processing scheme is shown in figure 1.

### 2.4. Characterization

The morphology of the AgNWs and AgNPs were characterized using a Phenom desktop SEM (15 kv, Pro X, Phenom). The thickness of nanocomposites was characterized using TMA (Q400, TA universal) with an expansion probe at room temperature. Weight percentage was obtained by burning the nanocomposite with a TGA (Q500, TA universal) and then converted to volume percentage. The electrical conductivity of thin films was measured using the four-probe method (Loresta-GP MCP-T610). The wide-angle x-ray diffraction (WAXD, Smartlab x-ray diffractometer, Rigaku) was used to characterize the nanofiller crystallinity, and small-angle diffraction (2D-XRD, Oxford Diffraction Xcalibur 3 x-ray diffractometer) patterns were used to determine the orientation of thin films [47].

### 2.5. Numerical method

The simulation consisted of two steps. The first step was to construct the 3D geometry of the thin film and randomly generate the nanoparticle inside. The second step was to analyze the network after all nanoparticles were generated. The quantum tunneling effect was considered as the main factor affecting electrical conductivity [46, 48]. The length of a junction between nanofillers determined if the wire or particle was connected to the network. It was assumed that nanofillers could not cross each other. The shape of AgNWs was considered a cylinder, and the shape of AgNP was considered a sphere. According to the measurement of Ag nanoparticle and Ag nanowire, the parameters of two nanofillers were set as follows in the simulation. The diameter of each AgNW was 150 nm. The average length of AgNW is 18 $\pm$ 5 $\mu$m, so the length of AgNW was any value between 13 to 23 $\mu$m. The geometry of every AgNP was about a 200 nm diameter sphere. The simulation was carried out with MatLab [39].

The minimal length between two nanofillers was calculated and determined as the key parameter for analyzing the network. The minimum distance function (equation (1)) was applied in the calculation. The parameter V and W in the function was the two-point on the nanowire axis segment, shown in figure 2.

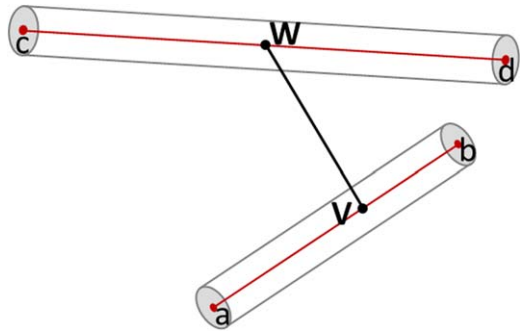


**Figure 2.** Minimal distance calculation.

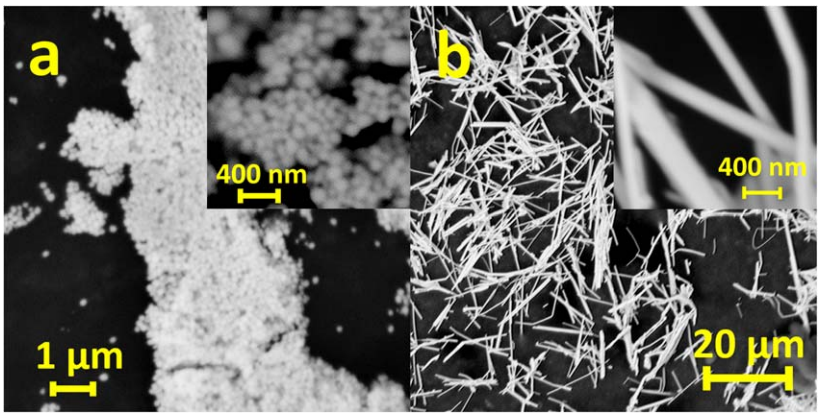


**Figure 3.** SEM images of (a) AgNP and (b) AgNW nanofiller.

$$a, b, c, d, V, W \in R^n$$
$$v, w \in R$$

$$V = \{v \times b + (1 - v) \times a | 0 \leqslant v \leqslant 1\}$$
$$W = \{w \times b + (1 - w) \times a | 0 \leqslant w \leqslant 1\}$$

$$\text{The distance of}(V, W) = \sqrt{\sum_{n}^{i=1}(v \times b_i + (1 - v) \times a_i - w \times c_i - (1 - w) \times d_i)^2} \quad (1)$$

In order to ensure every particle or wire was compliant with the rules, the flow chart was shown in the source file, figure s1 (available online at stacks.iop.org/NANOX/2/010019/mmedia). The primary purpose of analyzing the network was to determine if a conductive network was formed or not.

## 3. Results and discussion

### 3.1. Morphology

Figure 3 showed the image of AgNP (figure 3(a)) and AgNW (figure 3(b)). The average size of a single AgNP was 200 nm. AgNW had an average length, and the diameter was 18 $\pm$ 5 $\mu$m and 150 nm. As observed via SEM, the aggregation of silver nanofiller was distinct because the nanofiller was stored in acetone [49]. After sonication and mixing with DMF, most large aggregates were eliminated. In order to eliminate unfavorable aggregation, nanofillers were used right after being synthesized. However, the AgNP would still disperse as small aggregate in the polymer solution, shown in source file figure s4.

The electrical network was dictated by the silver nanofiller's dispersion in PAN. A careful inspection of the nanocomposite at different vol% was critical in understanding the percolation formation. Figures 4(a) and (b) showed the surface of AgNP/PAN at 7 vol% and 18 vol%. Most AgNPs were embedded in the polymer matrix. As vol% increased, the number of AgNPs increased visibly. Meanwhile, there was no electrically conductive network observed at 18 vol%. A closer inspection of the AgNP/PAN revealed less interaction among particles, shown in figure 4(a). Figures 4(c) and (d) showed the surface of PAN/AgNW at 9 vol% and 17 vol%. In those

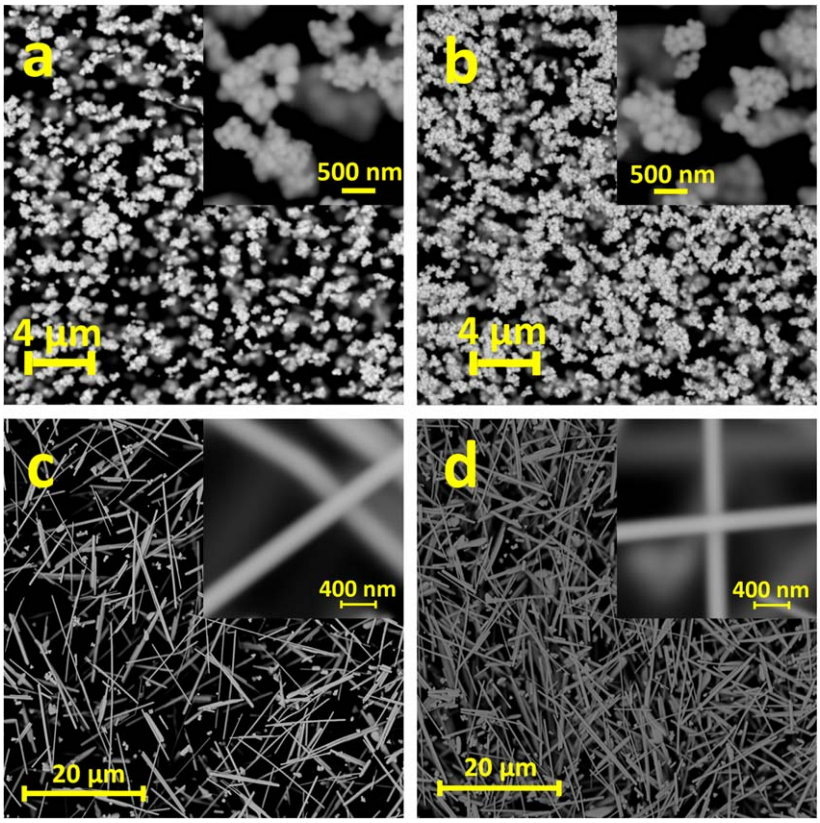


**Figure 4.** SEM images of (a) 7 vol% AgNP/PAN, (b) 18 vol% AgNP/PAN, (c) 9 vol% AgNW/PAN, and (d) 17 vol% AgNW/PAN.

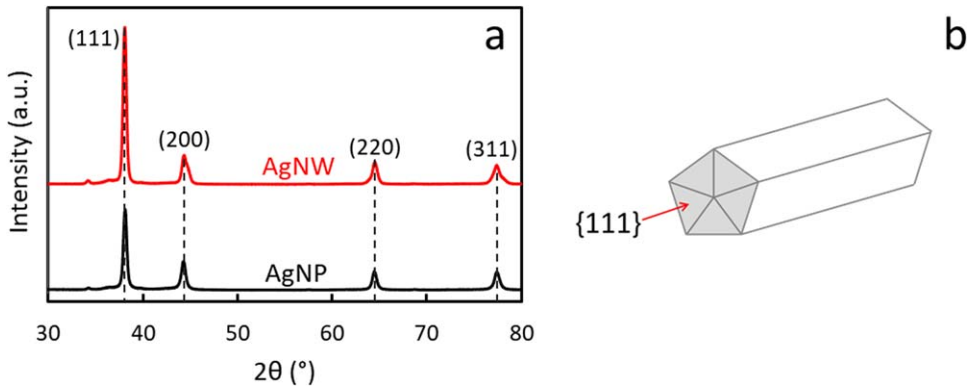


**Figure 5.** (a) XRD patterns, and (b) Illustration for AgNW growth.

figures, it could be observed that most AgNWs were separated, and aggregates were removed. At 9 vol%, the silver nanowires overlapped each other and formed a complete network. As vol% increased, the overlapping of each AgNW also increased, and the conductive network gradually formed. When vol% increased to 17 vol%, a complete nanowire network can be distinctly observed. The nanofillers' dispersion was evident.

The sample thickness was 6 $\mu$m, and the AgNWs were dispersed in three dimensions within the nanocomposite. Meanwhile, the spin coating process resulted in a smooth surface because the vertical nanowires would settle and flatten out during spinning. Most AgNWs were embedded in the PAN matrix. Only a small amount of AgNWs was exposed to the surface. As AgNWs were embedded tightly in cured PAN, which created an electrically conductive network.

### 3.2. XRD results

Since silver was the nanofiller, its orientation within the nanocomposite gave more insight into understanding its electric conductivity. The silver nanofillers were synthesized, and a wide-angle XRD was used to characterize

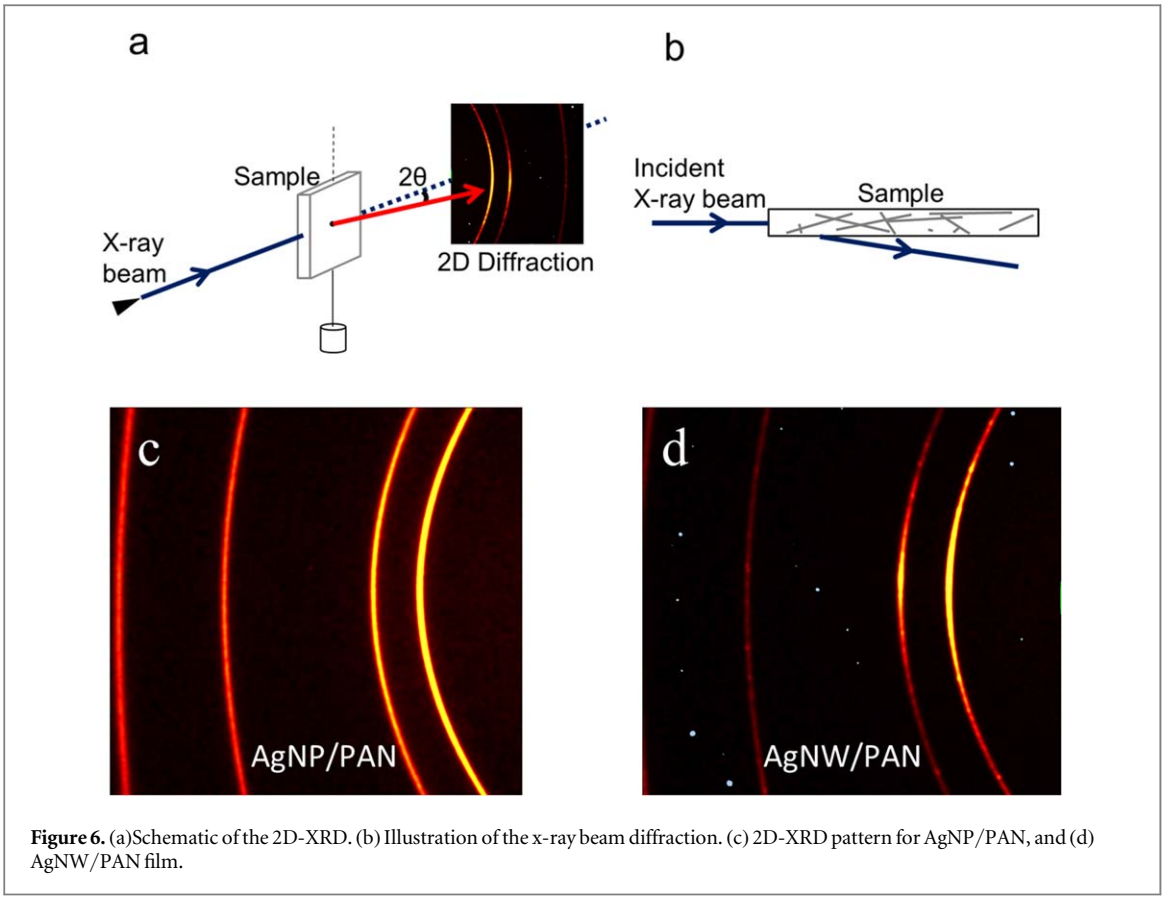


**Figure 6.** (a)Schematic of the 2D-XRD. (b) Illustration of the x-ray beam diffraction. (c) 2D-XRD pattern for AgNP/PAN, and (d) AgNW/PAN film.

the AgNP and AgNW nanofiller structure. In figure 5(a), the XRD results showed four prominent peaks corresponded to (111) at 38.1°, (200) at 44.4°, (220) at 64.5°, (311) at 77.4°, which agreed with a published report from Jyoti *et al* [50]. A very sharp (111) peak was evident at 38.1° for AgNP and AgNW. As more silver atoms attached to the (111) plane and AgNW grew in the [110] direction (figure 5(b)), high orientation was observed [51].

In order to prove the orientation of nanowires in the film, the incident x-ray was shot through the film (in-plane direction), and the 2D detector collected the diffracted information, shown in figures 6(a), (b). The AgNW was embedded in PAN after spinning. The average length of AgNW ($18 \pm 5\ \mu$m) was more than the thickness of derived nanocomposites (6 $\mu$m). In figure 6(d), distinct orientations were visible, which was influenced by the AgNW length, nanocomposite thickness, and the processing method. Compared to the AgNW sample, the ring of the AgNP sample (figure 6(c)) was continuous. The four arcs were attributed to the (111), (200), (220), (311) peak (shown in figure 5(a)). The intensity of each arc was confirmed with the XRD result, especially for AgNP. At a certain thickness of the film, far smaller than the length of the nanofiller, longer AgNW leads to a higher orientation.

### 3.3. Experimental electrical conductivity and modeling results

The film was thin (6 $\mu$m) and elastic. Peeling it from the slide could easily make a permanent deformation, affecting electrical conductivity [52]. So after the sample was taken out of the oven, further electrical measurements were conducted on the film slide. A four-point probe method was used to measure electrical conductivity. Measurements were conducted at five different places for each sample (and five times per place). The final conductivity was the average value of the data. Figure 7(a) showed the nanocomposites' electrical conductivity as a volume percentage for AgNW/PAN film. With TGA amended, the volume percentage of AgNW was from 9.2 to 18.6 vol%. As the 7 vol% AgNW/PAN film was not conductive, a sharp increase was observed from 9.2 to 10.6 vol%. It was possible to determine that 9.2 vol% was near the percolation threshold.

Moreover, percolation could be affected by wire distribution dispersion [53]. The percolation threshold was hard to find on the experimental result, but the trend was evident. The electrical conductivity measurement of 0.011 S $m^{-1}$ at 9.2 vol% suggested that a conductive network was established. Therefore, the percolation threshold should be below 9.2 vol%. Below the percolation threshold, the nanowires' concentration dominantly affects the percolation formation, thus the conductivity. After the percolation threshold, the tunneling effect mainly influences conductivity [54].

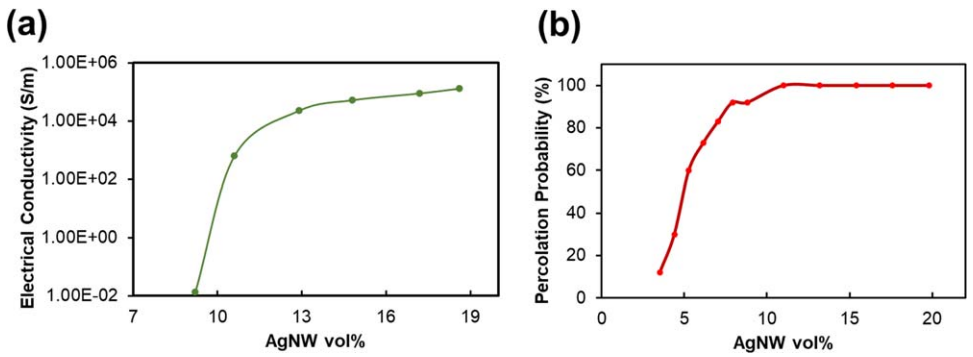


**Figure 7.** (a) Electrical conductivity at various volume percentages of AgNW. (b), Percolation probability Versus AgNW vol%.

A percolation probability simulation was used to understand the sharp change in conductivity better. Silver nanowires in the simulation volume were presented in the source file, figure s2. The results were collected from 600 simulations, 50 simulations for each vol%. In the simulation, the number of nanowires generated was determined by the volume percentage. The simulation results were shown in figure 7(b). As the number of nanowires increased, the percolation success probability increased. Only 12% of simulations showed percolation success at 3.5 vol%. At 7.0 vol%, 82% of simulations showed percolation success. 18% of the sample can be treated as an insulator. In other words, nanowires were partially networked at this amount, and some nanowires were still segregated. As vol% increased to 8.8 vol%, 92% of simulations showed percolation success. After generating more nanowires in the model, at 11 vol%, more conductive pathways were formed and resulted in high electrical conductivity. If more nanowires were added after this amount, more nanowires could be connected and would smoothly increase the electrical conductivity. Another finding could explain the sharp increase of conductivity: as the AgNW vol% increased linearly, the wire interactions increased exponentially, shown in the source file, figure s3. After the volume percentage exceeded 9 vol%, long connectivity was achieved, the intersections of the nanowires increased exponentially, which decreased the resistance. Overall, it is possible to conclude that the sharp change of electrical conductivity was mainly due to a percolation probability of 90% being achieved.

Compared to the AgNW/PAN film, the AgNP/PAN film was not conductive even at 29.6 vol%. A very low conductivity, which was 0.52 S $m^{-1}$, was measured at 54.4 vol% of AgNP/PAN. After increasing the AgNP volume to 61.9 vol%, the conductivity increased to 34.4 S $m^{-1}$, which was lower than AgNW/PAN film at 10.6 vol%. The lower conductivity of AgNP/PAN could be caused by the contact resistance between the particles [55, 56]. The contact resistance of the AgNP/PAN film was too high to be measured. Typically, smaller particle size results in a lower percolation threshold [52]. 200 nm AgNP used in this study was bigger than other studies that are focusing on AgNP based conductive nanocomposite [57, 58]. For example, Muhammed *et al* used 77 nm AgNP to make an electrically conductive nanocomposite fiber in their study [57]. It was hard to determine AgNP/PAN's percolation threshold from the experiment results because of the low conductivity. Therefore, we performed an aggregation theory based simulation for AgNP/PAN in the next section. However, there was a significant difference between AgNP/PAN and AgNW/PAN on conductivity. The effect of morphology on electrical conductivity was evident.

## 4. Influence of particle geometry

It is important to clarify how the geometry of particles affects the conductive network's formation. A mathematical model was established to understand the aggregation situations of nanoparticles in figure 8. We applied this model to explain the excellency of nanowire compared to the spherical nanoparticles, in other words, AgNW Versus AgNP. Experimental results showed that AgNP/PAN film could not achieve electrical conductivity until 15 vol%. However, the AgNW/PAN film could form a conductive network at 9 vol%. The property of nanoparticle-based nanocomposite was highly dependent on its aggregation structure. For example, a CB based high-structure could form a conductive network more efficiently than the low-structure one [59, 60]. However, the mathematical approach of the percolation mechanism was not well developed. Consequently, quality control and empirical methods were the only tools for the industry in production [61].

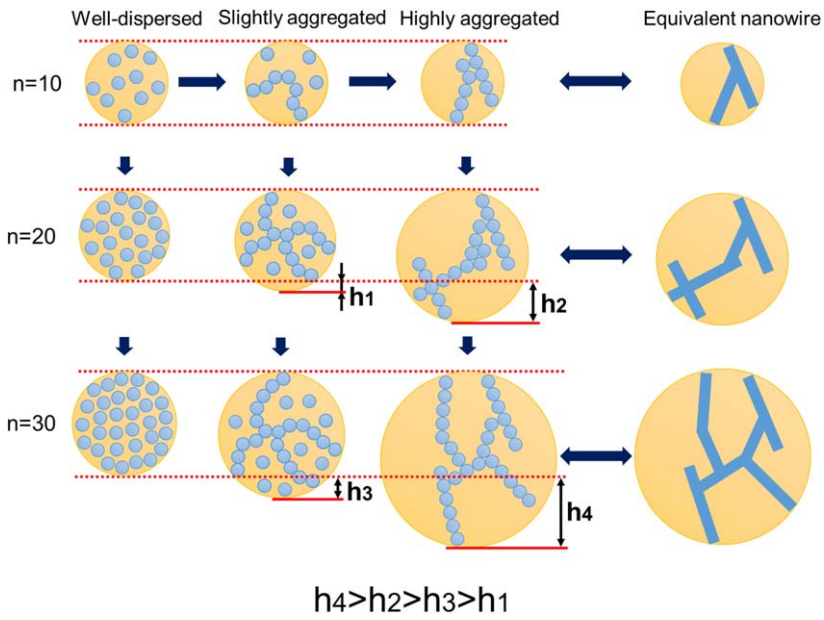


**Figure 8.** Evolution of aggregate model for well-dispersed, slightly-aggregated, highly-aggregated, and equivalent nanowire.

### 4.1. Conductive unit model

We established a model for understanding the formation efficiency of conductive networks, as illustrated in figure 8. We assumed the conductive network consists of similar units: the conductive unit (the yellow circle). In this case, a smaller conductive network based on the tunneling effect always existed inside this conductive unit. We assumed the number of conductive nanoparticles inside a single conductive unit was the same for a better comparison. From left to right, the degree of aggregation increased. Figure 8, from top to bottom, the number of nanoparticles increased.

For the well-dispersed conductive unit, particles were close to each other. As a result, this unit was conductive but not as efficient as other conformations. When slightly aggregated, some of the nanoparticles attracted each other and formed a dendritic structure. When the nanoparticles were highly aggregated, most nanoparticles attracted each other and formed a bar-like structure. While $n = 20$, the increments of size on three conductive units were different, the size of well-dispersed conductive units increased little, and the highly-aggregated aggregate increased the most. While $n = 30$, the difference in size increment between the three types of conductive units were much more dominant. The bars' structure in highly aggregated conductive units could be regarded as nanowire, and the conductive units were like a low aspect ratio nanowire cluster. This phenomenon could be concluded as the following. The addition of nanoparticles was mostly 'wasted' everywhere in the well-dispersed scenario, and the size of the conductive unit changed little. The additional nanoparticles were attached to the branch for the slightly aggregated scenario, and the rest were dispersed. The size of the conductive unit changed more than the well-dispersed. The additional nanoparticles were attached straightly on the formed bars for the highly aggregated scenario or form new bars. In both ways, the size of the conductive unit was significantly increased. As shown in figure 8, the excess part's size was defined as 'h' and the $h_4 > h_2 > h_3 > h_1$. With the number of nanoparticles increases, the aggregate size was dominantly affected by the aggregation degree.

Based on this model, with the same number of particles, the highly aggregated conductive unit trends to be larger. For a certain size, the highly-aggregated conductive unit needed fewer particles to form a conductive network inside. Furthermore, with the same size of the conductive unit, the highly-aggregated conductive unit tended to form a larger conductive network in the nanocomposite. Nanowire could be considered as a special case of the highly-aggregated conductive unit. For example, the silver nanowire aspect ratio was over 100 in this study, and the AgNW could be regarded as 100 stacked AgNP. Practically, the AgNW nanocomposite achieved electrical conductivity at a lower threshold than the AgNP nanocomposite [61].

### 4.2. Simulation on aggregation

In figure 4(a), the irregular shape of the AgNP aggregates was evident. They may cause some anisotropic property and eventually influence network formation. Generally, the silver nanoparticles have a percolation threshold of around 5 to 20 vol% [61]. Therefore, the simulation of 20 vol% of AgNP/PAN was used to study the influence of aggregate geometry on the percolation. As the previous section mentioned, the diameter of AgNP

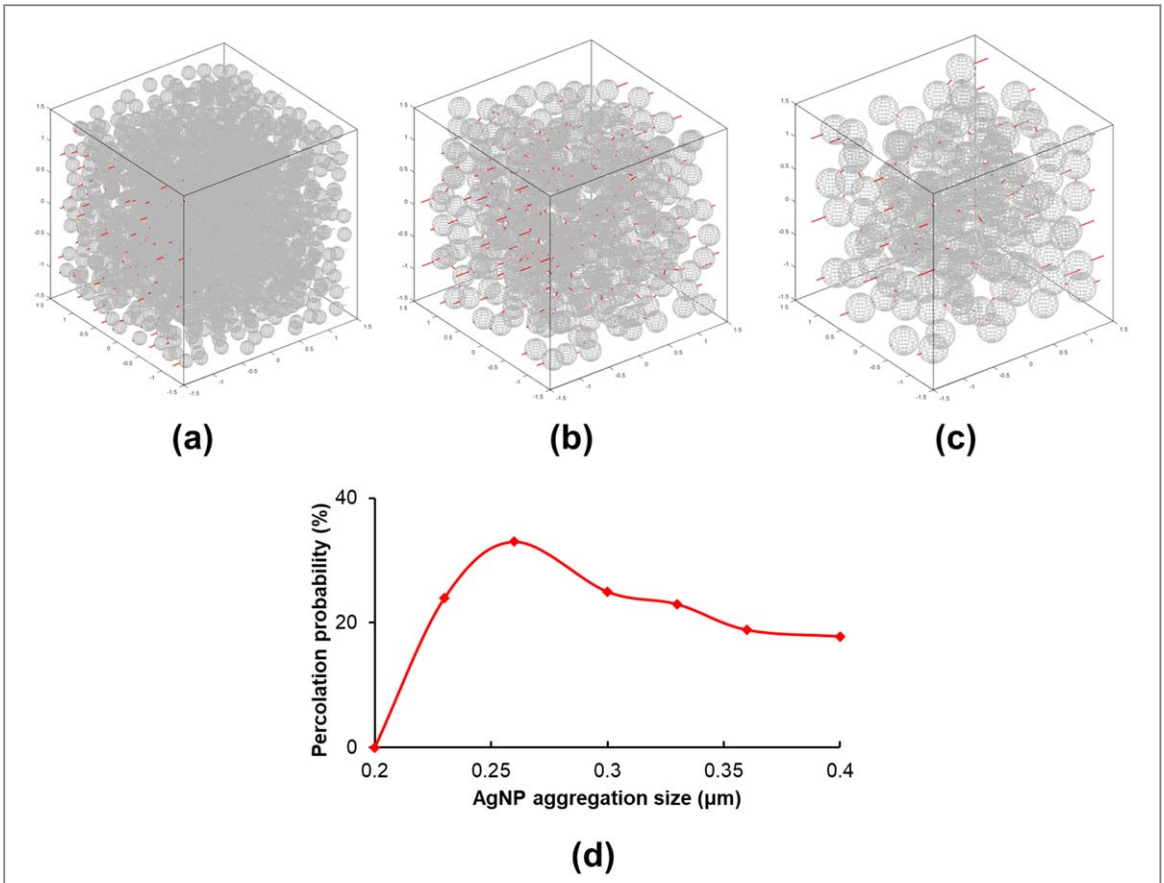


**Figure 9.** Simulation of aggregates size is (a) 0.2 $\mu$m, (b) 0.3 $\mu$m, and (c) 0.4 $\mu$m, (d) AgNP aggregation size Versus percolation success.

was 0.2 $\mu$m. In the first 100 simulations, we considered the silver nanoparticles were very well dispersed, and every particle stayed alone in the $3 \times 3 \times 3$ cube, and 1289 particles were generated, as shown in figure 9(a). The red bar in the cube represented the directly connected particle. With AgNW/PAN's experimental data, a valid connection was considered as the distance between each particle was smaller than 0.03 $\mu$m. No percolation was shown after 100 simulations.

For the 100 simulations shown in figure 9(b), we considered the nanoparticles formed irregular shape aggregates, and the average size of the aggregates is 0.3 $\mu$m. In order to have 20 vol% AgNP in the cube, the particle volume was expanded 3.375 times compare to 0.2 $\mu$m particle's, and the generating particle number decreased to 382. Even as little as two silver particles can form an irregular aggregation, it will increase the real particle number. In order to simplify the simulation, the least particle number was used. In figure 9(b), each particle in the cube was considered to be a 0.3 $\mu$m irregular aggregate. 25 of 100 simulations showed successful percolation. Interestingly, after each irregular aggregate's size increased to 0.4 $\mu$m, only 18 of 100 simulations showed successful percolation. A percolation of 0.4 $\mu$m silver aggregates was shown in figure 9(c). More simulations on various AgNP aggregation sizes were made, and the trend was obtained. Out of 100 simulations, the percolation probability dramatically increased first and then decreased with the aggregates' size increased, shown in figure 9(d). The percolation probability reached the maximum value 33% at 0.26 $\mu$m and then decreased to 18% at 0.4 $\mu$m.

With the increase of successful percolation followed, the increase of conductive unit size could be expounded. First, with the anisotropism of the conductive unit, the difficulties in forming a conductive network decreased. Second, based on our model, the size of the conductive unit increased little. It required less conductive unit for a conductive network, which implied the network's formation more efficiently. However, the effect of the anisotropic property was dominant at this scale. With the aggregation size increased, the nanoparticle aggregate needed more nanoparticles to fill the space. As a result, the size of the conductive unit increased a little bit. The decrease of successful conductive simulation could be explained as the aggregate number decrease became much influential. Thus, bigger nanoparticle aggregates would increase the difficulty in forming a conductive network.

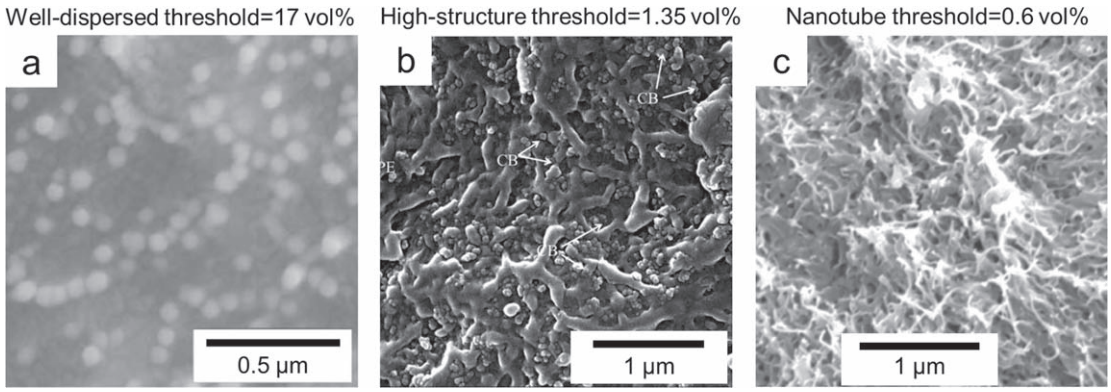


**Figure 10.** SEM image of (a)well dispersed structure of AgNP/HDPE nanocomposite. Reprinted from [62], Copyright (2010), with permission from Elsevier. ; (b) high structure of CB/HDPE nanocomposite [59] John Wiley & Sons. © 2013 Wiley Periodicals, Inc.; (c) nanotube connection of CNT/PLLA nanocomposite. Reproduced from [63] with permission of The Royal Society of Chemistry.

### 4.3. Validation of the model

The extension of this model confirmed previous studies well. For instance, electrical conductivity evolved differently with three distinct particle morphologies, as shown in figure 10: well-dispersed nanoparticle, high structure nanoparticle, and nanowire. In the well-dispersed scenario, more nanoparticles were consumed to extend the conductive unit size. Therefore, the conductive threshold of AgNP/HDPE nanocomposites in figure 10(a) is as high as 17 vol% (~68 wt%) [62]. CB aggregates were aggregated into high-structure in figure 10(b). Expanding the size of conductive units would consume fewer particles. The CB/HDPE had a low threshold of 2.7 wt% (1.35 vol%) [59]. In figure 10(c), the conductive threshold of CNT/PLLA nanocomposite was as low as 0.6 vol% (1.2 wt%) [63]. The nanotube consumed the least 'nanoparticles' to extend the conductive unit size. In conclusion, particles' geometry had a significant effect on affecting network formation, and our model provided a novel insight into this subject.

## 5. Conclusions

In this study, AgNW/PAN and AgNP/PAN were characterized, and differences were observed in the percolation behavior. These differences were attributed to the nanofiller geometry. The experimental result showed that the electrical conductivity increased with the volume percentage increase above 9.2 vol% for AgNW/PAN. The percolation threshold for AgNW/PAN was around 8–9 vol%. The AgNP/PAN exhibited a very low conductivity at 55 vol%. This result was expected because the larger size of AgNP would have a higher critical volume fraction, and the contact resistance between AgNP was very high.

For both nanocomposites, the simulation results agreed with the experimental data. Depending on the simulation result, the sharp increase in conductivity after the percolation threshold seems mainly affected by the increasing percolation probability and exponential increase of wire intersections. Another important finding was that the geometry of the aggregation of AgNP was the dominant factor in altering the percolation. The irregular shape of the aggregates would add an anisotropic property to the nanocomposites. As the size of the aggregates increased, the number of aggregates decreased at a certain concentration. By increasing the critical fraction, the formation of the conductive network was hindered. A conductive unit based geometrical model was established to understand the complex aggregation behavior of nanoparticles. Such a model was successfully applied to explain the experimental and simulation results.

## Acknowledgments

We gratefully thank Yangjie Qi (Department of Computer and Electrical Engineering, University of Dayton) and Chang Liu (Lerner Research Institute, Cleveland Clinic Foundation) for their help in the simulation.

## Data availability statement

The data that support the findings of this study are available upon reasonable request from the authors.

## Notes

The authors declare no competing interests.

## ORCID iDs

Qichen Fang https://orcid.org/0000-0002-7732-7672

## References

[1] Walker S B and Lewis. J A 2012 Reactive silver inks for patterning high-conductivity features at mild temperatures *JACS* **134** 1419–21
[2] Alshehri A H, Jakubowska M, Młoz˙niak A, Horaczek M, Rudka D, Free C and Carey J D 2012 Enhanced electrical conductivity of silver nanoparticles for high frequency electronic applications *ACS applied Materials & Interfaces* **4** 7007–10
[3] Zhan C, Yu G, Lu Y, Wang L, Wujcik E and Wei S 2017 Conductive polymer nanocomposites: a critical review of modern advanced devices *J. Mater. Chem. C* **5** 1569–85
[4] Amjadi M, Pichitpajongkit A, Lee S, Ryu S and Park I 2014 Highly stretchable and sensitive strain sensor based on silver nanowire–elastomer nanocomposite *ACS nano* **8** 5154–63
[5] Min S H, Asrulnizam A M, Atsunori M and Mariatti M 2019 Properties of stretchable and flexible strain sensor based on silver/PDMS nanocomposites *Mater. Today Proc.* **17** 616–22
[6] Wanekaya A K, Chen W, Myung N V and Mulchandani A 2006 Nanowire-based electrochemical biosensors *Electroanalysis: An International Journal Devoted to Fundamental and Practical Aspects of Electroanalysis* **18** 533–50
[7] Altin Y, Tas M, Borazan İ, Demir A and Bedeloglu A 2016 Solution-processed transparent conducting electrodes with graphene, silver nanowires and PEDOT: PSS as alternative to ITO *Surf. Coat. Technol.* **302** 75–81
[8] Mohammadnezhad M, Gurpreet Singh Selopal N, Alsayyari R, Akilimali F, Navarro-Pardo Z M, Wang B, Stansfield H, Zhao and Rosei F 2018 CuS/graphene nanocomposite as a transparent conducting oxide and pt-free counter electrode for dye-sensitized solar cells *J. Electrochem. Soc.* **166** H3065
[9] Yuksel R, Coskun S, Gunbas G, Cirpan A, Toppare L and Unalan H E 2017 Silver nanowire/conducting polymer nanocomposite electrochromic supercapacitor electrodes *J. Electrochem. Soc.* **164** A721
[10] Wadhwa H, Kumar D, Mahendia S and Kumar S 2017 Microwave assisted facile synthesis of reduced graphene oxide-silver (RGO-Ag) nanocomposite and their application as active SERS substrate *Mater. Chem. Phys.* **194** 274–82
[11] Ackermann T, Sahakalkan S, Kolaric I, Westkämper E and Roth S 2015 Technical requirements, manufacturing processes and cost efficiency for transparent electrodes based on silver nanowires and carbon nanotubes In*Nanoengineering: Fabrication, Properties, Optics, and Devices XII* **9556** 955602 International Society for Optics and Photonics
[12] Song M *et al* 2013 Highly efficient and bendable organic solar cells with solution-processed silver nanowire electrodes *Adv. Funct. Mater.* **23** 4177–84
[13] Li B, Ye S, Stewart I E, Alvarez S and Wiley B J 2015 Synthesis and purification of silver nanowires to make conducting films with a transmittance of 99% *Nano Lett.* **15** 6722–6
[14] Zhang Y, Guo J, Xu D, Sun Y and Yan F 2017 One-pot synthesis and purification of ultralong silver nanowires for flexible transparent conductive electrodes *ACS Appl. Mater. Interfaces* **9** 25465–73
[15] Cho S, Kang S, Pandya A, Shanker R, Khan Z, Lee Y, Park J, Craig S L and Ko H 2017 Large-area cross-aligned silver nanowire electrodes for flexible, transparent, and force-sensitive mechanochromic touch screens *Acs Nano* **11** 4346–57
[16] Ricciardulli A, Gaetano S, Yang G - J A H, Wetzelaer X, Feng and Blom P W M 2018 Hybrid silver nanowire and graphene-based solution-processed transparent electrode for organic optoelectronics *Adv. Funct. Mater.* **28** 1706010
[17] Korte K E, Sara E S and Xia Y 2008 Rapid synthesis of silver nanowires through a CuCl-or CuCl 2-mediated polyol process *J. Mater. Chem.* **18** 437–41
[18] Sun Y, Gates B, Mayers B and Xia Y 2002 Crystalline silver nanowires by soft solution processing *Nano Lett.* **2** 165–8
[19] Tao A, Sinsermsuksakul P and Yang P 2006 Polyhedral silver nanocrystals with distinct scattering signatures *Angew. Chem. Int. Ed.* **45** 4597–601
[20] Wiley B, Sun Y, Mayers B and Xia Y 2005 Shape-controlled synthesis of metal nanostructures: the case of silver *Chemistry–A European Journal* **11** 454–63
[21] Ran, Yunxia W H, Wang K, Ji S and Ye C 2014 A one-step route to Ag nanowires with a diameter below 40 nm and an aspect ratio above 1000 *Chem. Commun.* **50** 14877–80
[22] Sun Y, Yin Y, Mayers B T, Herricks T and Xia Y 2002 Uniform silver nanowires synthesis by reducing AgNO3 with ethylene glycol in the presence of seeds and poly (vinyl pyrrolidone) *Chem. Mater.* **14** 4736–45
[23] Lee J, Lee P, Lee H, Lee D, Lee S S and Ko S H 2012 Very long Ag nanowire synthesis and its application in a highly transparent, conductive and flexible metal electrode touch panel *Nanoscale* **4** 6408–14
[24] Wiley B, Herricks T, Sun Y and Xia Y 2004 Polyol synthesis of silver nanoparticles: use of chloride and oxygen to promote the formation of single-crystal, truncated cubes and tetrahedrons *Nano Lett.* **4** 1733–9
[25] Wiley B, Sun Y and Xia Y 2005 Polyol synthesis of silver nanostructures: control of product morphology with Fe (II) or Fe (III) species *Langmuir* **21** 8077–80
[26] Zhang P, Wyman I, Hu J, Lin S, Zhong Z, Tu Y, Huang Z and Wei Y 2017 Silver nanowires: synthesis technologies, growth mechanism and multifunctional applications *Materials Science and Engineering: B* **223** 1–23
[27] Agnihotri S, Mukherji S and Mukherji S 2014 Size-controlled silver nanoparticles synthesized over the range 5–100 nm using the same protocol and their antibacterial efficacy *RSC Adv.* **4** 3974–83
[28] Bastús N G, Merkoçi F, Piella J and Puntes V 2014 Synthesis of highly monodisperse citrate-stabilized silver nanoparticles of up to 200 nm: kinetic control and catalytic properties *Chem. Mater.* **26** 2836–46
[29] Hulteen J C, Treichel D A, Smith M T, Duval M L, Jensen T R and Van Duyne R P 1999 Nanosphere lithography: size-tunable silver nanoparticle and surface cluster arrays *The Journal of Physical Chemistry* **B103** 3854–63
[30] Wang S, Tian Y, Ding S and Huang Y 2016 Rapid synthesis of long silver nanowires by controlling concentration of Cu2 + ions *Mater. Lett.* **172** 175–8

[31] Ma J and Zhan M 2014 Rapid production of silver nanowires based on high concentration of $AgNO_3$ precursor and use of FeCl 3 as reaction promoter *RSC Adv.* **4** 21060–71
[32] Zhang K, Du Y and Chen S 2015 Sub 30 nm silver nanowire synthesized using KBr as co-nucleant through one-pot polyol method for optoelectronic applications *Org. Electron.* **26** 380–5
[33] De S, Higgins T M, Lyons P E, Doherty E M, Nirmalraj P N, Blau W J, Boland J J and Coleman J N 2009 Silver nanowire networks as flexible, transparent, conducting films: extremely high DC to optical conductivity ratios *ACS nano* **3** 1767–74
[34] Al-Ajrash,, Nabat S M, Lafdi K, Vasquez E S, Chinesta F and Coustumer P L 2018 Experimental and numerical investigation of the silicon particle distribution in electrospun nanofibers *Langmuir* **34** 7147–52
[35] Liu C, Sergeichev I, Akhatov I and Lafdi K 2018 CNT and polyaniline based sensors for the detection of acid penetration in polymer composite *Compos. Sci. Technol.* **159** 111–8
[36] Liu C, Lafdi K and Chinesta F 2020 Durability sensor using low concentration carbon nano additives *Compos. Sci. Technol.* **195** 108200
[37] Liu C and Lafdi K 2019 Self-assembly and surface tension induced fractal conductive network in ternary polymer system *ACS Applied Polymer Materials* **1** 493–9
[38] Sadeghi S, Arjmand M, Navas I O, Yazdi A Z and Sundararaj U 2017 Effect of nanofiller geometry on network formation in polymeric nanocomposites: Comparison of rheological and electrical properties of multiwalled carbon nanotube and graphene nanoribbon *Macromolecules* **50** 3954–67
[39] Nuha A H, Liu C, Dumuids J-B and Lafdi K 2016 Intelligent design of conducting network in polymers using numerical and experimental approaches *RSC Adv.* **6** 95010–20
[40] Jiang H, Moon K-S, Li Y and Wong C P 2006 Surface functionalized silver nanoparticles for ultrahigh conductive polymer composites *Chem. Mater.* **18** 2969–73
[41] Ackermann T, Neuhaus R and Roth S 2016 The effect of rod orientation on electrical anisotropy in silver nanowire networks for ultra-transparent electrodes *Sci. Rep.* **6** 34289
[42] Davidson E R 2000 Computational Transition Metal Chemistry *Chemicl Reviews* **100.2** 351–2
[43] Yang X, Hu J, Chen S and He J 2016 Understanding the percolation characteristics of nonlinear composite dielectrics *Sci. Rep.* **6** 30597
[44] Morishita T, Matsushita M, Katagiri Y and Fukumori K 2011 A novel morphological model for carbon nanotube/polymer composites having high thermal conductivity and electrical insulation *J. Mater. Chem.* **21** 5610–4
[45] Bao W S, Meguid S A, Zhu Z H and Weng G J 2012 Tunneling resistance and its effect on the electrical conductivity of carbon nanotube nanocomposites *J. Appl. Phys.* **111** 093726
[46] Suh D, Faseela K P, Kim W, Park C, Lim J G, Seo S, Kim M K, Moon H and Baik S 2020 Electron tunneling of hierarchically structured silver nanosatellite particles for highly conductive healable nanocomposites *Nat. Commun.* **11** 1–11
[47] Rodriguez-Navarro A B 2006 XRD2DScan: new software for polycrystalline materials characterization using two-dimensional x-ray diffraction *J. Appl. Crystallogr.* **39** 905–9
[48] Vodolazskaya I V, Andrei V E, Akhunzhanov R K and Tarasevich Y Y 2019 Effect of tunneling on the electrical conductivity of nanowire-based films: computer simulation within a core–shell model *J. Appl. Phys.* **126** 244903
[49] Tilaki R M and Mahdavi S M 2006 Stability, size and optical properties of silver nanoparticles prepared by laser ablation in different carrier media *Appl. Phys. A* **84** 215–9
[50] Jyoti K, Baunthiyal M and Singh A 2016 Characterization of silver nanoparticles synthesized using urtica dioica Linn. leaves and their synergistic effects with antibiotics *Journal of Radiation Research and Applied Sciences* **9** 217–27
[51] Yoo D-H, Cuong T V, Luan V H, Khoa N T, Kim E J, Hur S H and Hahn S H 2012 Photocatalytic performance of a Ag/ZnO/CCG multidimensional heterostructure prepared by a solution-based method *The J. Phys. Chem. C* **116** 7180–4
[52] D'Alessandro A, Materazzi A L and Ubertini F 2019 *Nanotechnology in cement-based construction* (Boca Raton: Jenny Stanford Publishing) S.l.: Pan Stanford Publishing (https://doi.org/10.1201/9780429328497)
[53] Al-Saleh M H and Sundararaj U 2009 A review of vapor grown carbon nanofiber/polymer conductive composites *Carbon* **47** 2–22
[54] Han B, Ding S and Yu X 2015 Intrinsic self-sensing concrete and structures: a review *Measurement* **59** 110–28
[55] Zhang R, Lin W, Moon K-S and Wong C P 2010 Fast preparation of printable highly conductive polymer nanocomposites by thermal decomposition of silver carboxylate and sintering of silver nanoparticles *ACS Appl. Mater. Interfaces* **2** 2637–45
[56] Zhang R, moon K-sik, Lin W and Wong C P 2010 Preparation of highly conductive polymer nanocomposites by low temperature sintering of silver nanoparticles *J. Mater. Chem.* **20** 2018–23
[57] Liu J, Li X and Zeng X 2010 Silver nanoparticles prepared by chemical reduction-protection method, and their application in electrically conductive silver nanopaste *J. Alloys Compd.* **494** 84–7
[58] Ajmal C M, Bae S and Baik. S 2019 A superior method for constructing electrical percolation network of nanocomposite fibers: *In situ* thermally reduced silver nanoparticles *Small* **15** 1803255
[59] Ren D, Zheng S, Wu F, Yang W, Liu Z and Yang M 2014 Formation and evolution of the carbon black network in polyethylene/carbon black composites: Rheology and conductivity properties *J. Appl. Polym. Sci.* **131** 39953
[60] Chen J, Cui X, Sui K, Zhu Y and Jiang W 2017 Balance the electrical properties and mechanical properties of carbon black filled immiscible polymer blends with a double percolation structure *Compos. Sci. Technol.* **140** 99–105
[61] Wypych G 2016 5-physical properties of fillers & filled materials *Handbook of Fillers* 4th (Toronto: ChemTec Publishing) 303–71
[62] Rybak A, Boiteux G, Melis F and Seytre G 2010 Conductive polymer composites based on metallic nanofiller as smart materials for current limiting devices *Compos. Sci. Technol.* **70** 410–6
[63] Zhang K *et al* 2017 Ultralow percolation threshold and enhanced electromagnetic interference shielding in poly (L-lactide)/multi-walled carbon nanotube nanocomposites with electrically conductive segregated networks *J. Mater. Chem. C* **5** 9359–69